



**HAL**  
open science

## Turbulent route to two-dimensional soft crystals

Mohit Gupta, Pinaki Chaudhuri, Jérémie Bec, Samriddhi Sankar Ray

► **To cite this version:**

Mohit Gupta, Pinaki Chaudhuri, Jérémie Bec, Samriddhi Sankar Ray. Turbulent route to two-dimensional soft crystals. *Physical Review E*, 2022, 106 (6), pp.L062601. 10.1103/PhysRevE.106.L062601 . hal-02362959

**HAL Id: hal-02362959**

**<https://hal.science/hal-02362959v1>**

Submitted on 3 Sep 2024

**HAL** is a multi-disciplinary open access archive for the deposit and dissemination of scientific research documents, whether they are published or not. The documents may come from teaching and research institutions in France or abroad, or from public or private research centers.

L'archive ouverte pluridisciplinaire **HAL**, est destinée au dépôt et à la diffusion de documents scientifiques de niveau recherche, publiés ou non, émanant des établissements d'enseignement et de recherche français ou étrangers, des laboratoires publics ou privés.

# Turbulent Route to Two-Dimensional Soft Crystals

Mohit Gupta,<sup>1,2,\*</sup> Pinaki Chaudhuri,<sup>3,†</sup> Jérémie Bec,<sup>4,5,‡</sup> and Samriddhi Sankar Ray<sup>1,§</sup>

<sup>1</sup>International Centre for Theoretical Sciences, Tata Institute of Fundamental Research, Bangalore 560089, India

<sup>2</sup>School of Physics and Astronomy, University of Minnesota, Minneapolis, Minnesota 55455, USA

<sup>3</sup>The Institute of Mathematical Sciences, CIT Campus, Taramani, Chennai 600 113, India

<sup>4</sup>Université Côte d'Azur, Inria, CNRS, Cemeef, Sophia-Antipolis, France.

<sup>5</sup>MINES ParisTech, PSL Research University, CNRS, CEMEF, Sophia-Antipolis, France

We investigate the effect of a two-dimensional, incompressible, turbulent flow on soft granular particles and show the emergence of a crystalline phase due to the interplay of Stokesian drag and short-range inter-particle interactions. We quantify this phase through the bond order parameter and local density fluctuations and find a sharp transition between the crystalline and non-crystalline phase as a function of the Stokes number. Furthermore, the nature of preferential concentration, characterised by the correlation dimension, is significantly different from that of particle-laden flows in the absence of repulsive potentials.

The self-assembly of particles in a flow [1, 2], because of its ubiquity, is amongst the most studied problem in the areas of turbulent transport, soft matter, granular systems and nonequilibrium statistical mechanics. In quiescent form, most dilute assemblies are liquids, which when densified, can take a crystalline or amorphous structure depending upon the dispersity of the constituents [3–6]. Consequently, extensive studies of the rheology of such suspensions have happened [7, 8], motivated by diverse applications. In typical experiments and computer simulations, the role of a carrier flow in dispersing the particulate matter is trivial: indeed if there is an underlying fluid medium, they are typically simple shearing [9, 10]. In a variety of natural and industrial processes, however, particles are dispersed in flows with non-trivial spatio-temporal correlations which are chaotic, and in extreme cases (such as a marine system) even turbulent [11–13].

This specific question of the structural properties of particulate suspension, where the underlying flow is turbulent, has surprisingly been not investigated despite significant progress in the last two decades in the area of turbulent transport of finite-sized, heavy, inertial (colloidal) particles. In this paper, we report the emergence of macroscopic particulate structures with crystalline (hexagonal) motifs even in the presence of strong mixing because of the carrier turbulent flow.

For suspended particles with a finite diameter and density, inertial effects and dissipative dynamics become important, leading to the particles detaching from the underlying flow to form strong inhomogeneities in their spatial distribution (see Fig. 1). This phenomenon, known as *preferential concentration*, has been extensively studied [14–19] and remains critical to our explanations of problems such as rain initiation in warm clouds. Al-

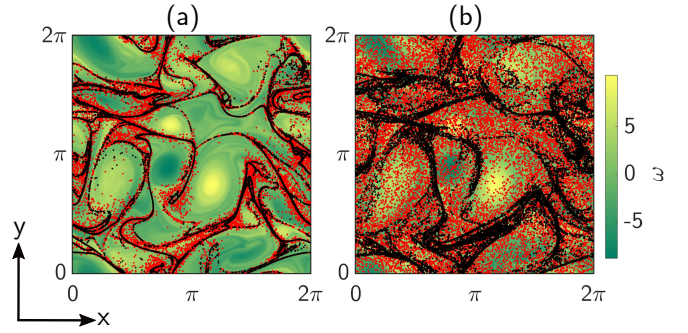


Figure 1.  $\phi = 0.1\%$ . Representative snapshots of non-interacting particles, i.e.  $V(r_{ij}) = 0$  (shown in black) and interacting soft particles (shown in red) with  $V(r_{ij})$  specified in Eqn.2, for Stokes numbers (a)  $St = 0.75$  and (b)  $St = 2.50$ , superimposed on vorticity field of the carrier turbulent flow.

though more recent studies have addressed the issue of effects such as gravity [20–22] and turbophoresis [23–25] on preferential concentration, inter-particle interactions have largely been ignored except for studies on coalescences [26, 27] and on Vicsek ordering [28]. The only example that we are aware of, which links ideas of soft matter and turbulent transport is the use of repulsive, elastic, hard sphere inter-particle interactions, which, combined with a dissipative dynamics, lead to *stickiness* and aggregation [29]. However, for most physical systems, the elastic limit is an idealised one: The most obvious particulate exchanges, such as those mediated through a *soft potential* [30] has been ignored so far.

In this work, we therefore address two important and related issues, namely what is the effect of soft particle interactions on clustering of particles in a turbulent flow and can such realistic interactions, contrary to naïve expectations, lead to the growth of stable crystalline structures in an ensemble of particles interacting with each other as well as an ambient turbulent fluid.

We consider an assembly of  $N_p$  particles seeded in a two-dimensional, statistically stationary, turbulent velocity field  $\mathbf{u}$  [31]. Since we consider particles smaller than

\* mohit.gupta9607@gmail.com

† pinakic@imsc.res.in

‡ Also: Associate, International Centre for Theoretical Sciences, Tata Institute of Fundamental Research, Bangalore 560089, India; jeremie.bec@mines-paristech.fr

§ samriddhisankarray@gmail.com

the relevant length scales of the flow, the dynamics of the  $i$ -th particle (characterised by its Stokes or particle response time  $\tau_p = \frac{2\rho_p a^2}{9\rho_f \nu}$ , where  $a$  is the particle radius,  $\nu$  the kinematic viscosity of the flow, and  $\rho_p$  and  $\rho_f$  are the particle and fluid densities, respectively) defined through its position  $\mathbf{x}_i$  and velocity  $\mathbf{v}_i$  is given by the linear Stokes drag model along with the inter-particle interaction potential  $V(r_{ij})$ :

$$\frac{d\mathbf{x}_i}{dt} = \mathbf{v}_i; \quad \frac{d\mathbf{v}_i}{dt} = -\frac{\mathbf{v}_i - \mathbf{u}(\mathbf{x}_i, t)}{\tau_p} - \sum_{\substack{j=1 \\ j \neq i}}^{N_p} \nabla V(r_{ij}); \quad (1)$$

where the interacting short-ranged repulsive potential [30, 32], commonly used for modelling emulsions and other soft granular suspensions, is given by:

$$V_{\text{soft}}(r_{ij}) = \begin{cases} \frac{\epsilon}{2}(1 - r_{ij}/\sigma_{ij})^2 & \text{for } r_{ij} < \sigma_{ij}, \\ 0 & \text{for } r_{ij} \geq \sigma_{ij}; \end{cases} \quad (2)$$

where,  $r_{ij}$  is the inter-particle separation,  $\sigma_{ij}$  is the sum of the radii of particles  $i$  and  $j$ ,  $\epsilon = 1$  sets the energy scale for particle interactions. Thus, such an interaction takes into account the energy cost of deformation, only when two particles are in contact. For our work, we mostly consider a mono-disperse assembly, where all particles have the same diameter  $\sigma$ . For the mono disperse suspensions, which is our focus, all particles have the same radius  $a$ ; hence  $\sigma = 2a$ . In the Supplemental Material [31] we show additional results for bi-disperse suspension where particles have different radii.

The advecting turbulent velocity  $\mathbf{u}$  is obtained (by using a standard pseudo-spectral method) as a solution of the two-dimensional, incompressible Navier-Stokes equation, written in the vorticity ( $\omega = \nabla \times \mathbf{u}$ ) formulation as

$$\partial_t \omega + \mathbf{u} \cdot \nabla \omega = \nu \nabla^2 \omega - \alpha \omega + \mathbf{f}; \quad (3)$$

with  $\nu$  the kinematic viscosity and  $\alpha$  Ekman friction coefficient. The flow is solved on a  $2\pi$  periodic grid with  $N = 512^2$  collocation points, and a deterministic large scale forcing  $f$ , ensuring a direct enstrophy cascade regime, maintains a non-equilibrium steady state [33]. The flow is conveniently described by its characteristic length  $l_\nu = \sqrt{\langle \Omega \rangle / \langle P \rangle} = 0.06$  and time  $\tau_f = \sqrt{1 / \langle \Omega \rangle} = 0.4$  scales, where  $\Omega = \int k^2 E(k) dk$  is the enstrophy and  $P = \int k^4 E(k) dk$  the palinstrophy [34]. We set the forcing length scale  $l_f = 1.71$  yielding a secondary time scale  $l_f / u_{\text{rms}} = 1.60$ ,  $u_{\text{rms}} = \sqrt{\int E(k) dk}$ . By using the flow time-scale, we define the non-dimensional Stokes number  $St = \tau_p / \tau_f$  and ensure that both the grid spacing and particle diameter are much smaller than  $l_\nu$ . Further, we vary the Stokes number by using different values of  $\tau_p$ .

The effect of such inter-particle interactions is striking. In Fig. 1 we show representative snapshots of particle positions, superimposed on the background vorticity field,

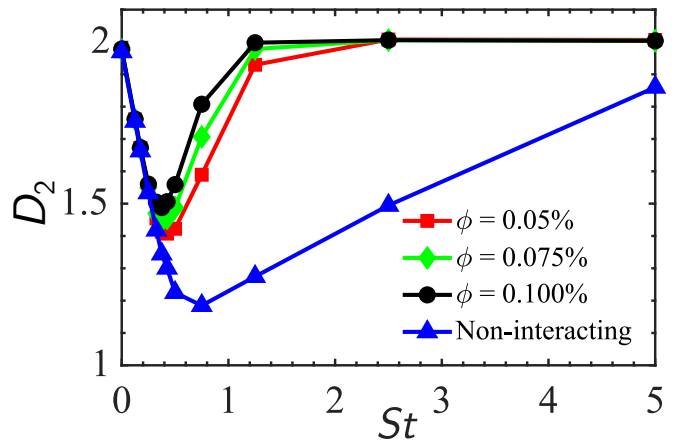


Figure 2. Correlation dimension  $D_2$  vs  $St$  for non-interacting (blue triangles) and interacting particles for ensembles for  $\phi$ , where  $N_p$  varies (see legend).

for both interacting (red) and non-interacting  $V(r_{ij}) = 0$  (black) particles. In the absence of inertia ( $St = 0$ ), unsurprisingly, the difference between the two ensembles is minute. However, for finite values of  $St$  (panels (a) and (b)), the particle distributions are strongly influenced by their interactions. In particular, the nature of small-scale clustering is significantly altered and, especially for  $St > 1$  (panel (b)), interacting particles appear to be more homogeneously distributed than the ones which are non-interacting.

Inhomogeneities in the particle distribution are conveniently characterized by the correlation dimension  $D_2$ , defined through the probability of having two particles within a distance  $r$ , namely  $P_2^<(r) \sim r^{D_2}$ , or equivalently through the small-scale behavior of the radial distribution function  $g(r) \sim r^{D_2-2}$ . Figure 2 shows  $D_2$  as a function of  $St$  (including in the non-interacting case), for various values of the packing fraction  $\phi = N_p \sigma^2 / (16\pi)$ . We fix  $\sigma = 5.0 \times 10^{-4}$ , and choose  $N_p = 1 \times 10^5$ ,  $1.5 \times 10^5$  and  $2.0 \times 10^5$ , to obtain  $\phi = 0.05\%$ ,  $0.075\%$  and  $0.10\%$ , respectively. For a given packing fraction and  $St \ll 1$ , the value of  $D_2$ , within error-bars, are indistinguishable from the non-interacting particles. This is because at such small values of  $St$ , there is hardly any small-scale clustering and therefore such dilute suspensions are only weakly affected by the short-range particulate interactions. However, as particles cluster, i.e. for  $St = \mathcal{O}(1)$ , soft granular repulsions dominate and, unlike the non-interacting ensemble, the interacting particles spread more—as a result of the competing interactions of vortical-ejection due to inertia and the short-range inter-grain repulsive energy cost—and with a larger value of  $D_2$ . This effect also leads to a slight shifting to the left of the value of  $St$  where  $D_2$  attains its minimum. This effect is of course accentuated with increasing packing fractions. For Stokes numbers a bit larger than 1, although the centrifugal vortical-ejection weakens, particles still tend to cluster in straining zones. However, the strength of the

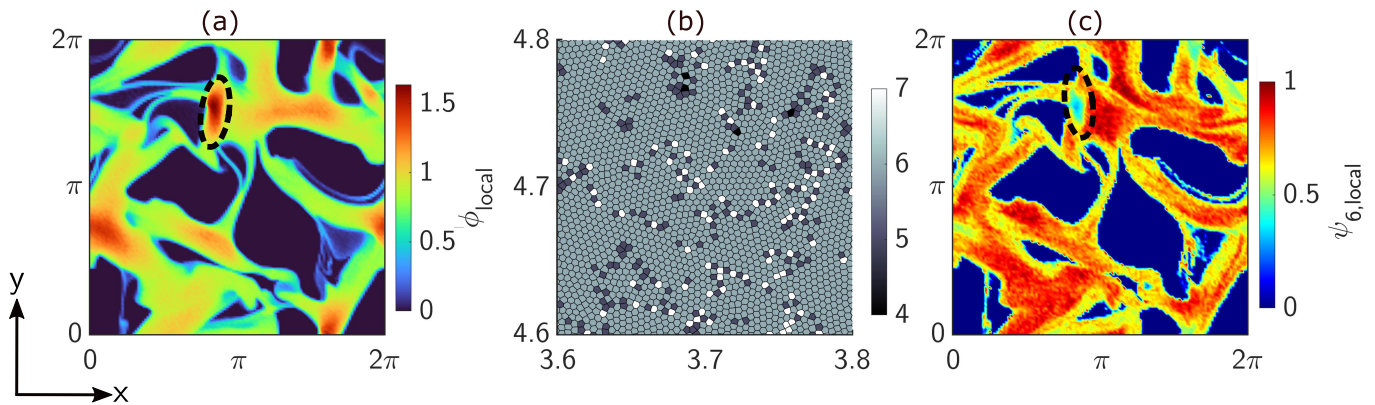


Figure 3.  $\phi = 50\%$ . (a) Local packing fraction field  $\phi_{\text{local}}$  for the suspended grains, with  $St \sim 1$ . The hyper packed region is highlighted by dashed black oval shape. (b) The Voronoi tessellation along with the coordination number  $z$  of each particle, shown as greyscale for a zoomed-in region having large  $\psi_{6,\text{local}}$ , points to strong evidence of crystalline order with a hexagonal packing. Color-bar shows number of sides of each Voronoi cell. (c) Corresponding map to panel (a) for the local bond order parameter  $\psi_{6,\text{local}}$  with re-entrant melting region highlighted by dashed black line. (See Refs. [35, 36] for an evolution of  $\phi_{\text{local}}$  and  $\psi_{6,\text{local}}$ .)

short-range repulsive forces ensure that interacting particles spread out more and sample the flow homogeneously, overcoming the bias due to inertia (Fig. 1(b)). We see evidence of this in our measurements, which show that for  $St > 1$  the correlation dimension  $D_2$  asymptotes to the physical dimension 2 much faster for the interacting than for the non-interacting case. Furthermore, the minimum value of  $D_2$  also increases as a function of  $\phi$ . Our results for packing fractions up to  $\phi = 50\%$  (see Fig. S1 in Ref. [31]) shows clearly that the minima in the correlation dimension becomes shallower and shallower; however it is a matter of speculation if the minima does not exist at even higher levels of packing.

Thus, as observed and discussed, inter-particle interactions in particle-laden turbulent flows clearly have an effect on the degree and nature of preferential concentration. But are such particle interactions strong enough to overcome turbulent mixing and nucleate crystalline structure? There are recent experimental studies which suggest that such aggregates may develop in homogeneous turbulence [37]. To answer this question—and provide compelling evidence—it is essential to work with a much larger packing fraction and particle diameter, as is common in studies of granular systems [38, 39]. (We however ensure that the diameters are still much smaller than the fluid characteristic length scale  $l_\nu$  for our model to be valid.) We therefore choose  $\sigma = 5 \times 10^{-3}$ , and different particle numbers, namely,  $N_p = 2 \times 10^5$  ( $\phi = 10\%$ ) and  $N_p = 10^6$  ( $\phi = 50\%$ ).

A useful indicator of how densely such particles are packed, due to inertia and interactions, is to look at the local packing fraction  $\phi_{\text{local}} = N_\Delta \pi \sigma^2 / (4\Delta^2)$ , where  $N_\Delta$  is the number of particles in a small square of side  $\Delta = 4\delta x$ , where  $\delta x$  is the width of our Eulerian grid. In Fig. 3(a) we show a representative pseudo-color snapshot of the local packing fraction for particles with  $St = 1$  ( $\phi = 50\%$ ). As we would expect, in a given snapshot,

there are regions which are extremely dense and the local packing fraction far exceeds its average  $\phi$ , with some regions hyper-packed due to the softness of the particles. We now examine the structure of these densely packed regions by using the standard approach of *Voronoi tessellation*. In Fig. 3(b) we show the Voronoi construction, corresponding to a zoomed-in region of panel (a); furthermore we color, on a greyscale, each cell by the coordination number  $z$  (values shown in the adjacent colorbar) of the particle. We find, surprisingly, that these soft particles do form hexagonal lattices, as suggested by the predominance of  $z = 6$  (light grey) and the cells of our Voronoi tessellation, with almost perfect crystalline order.

To quantify this degree of crystallinity, we use the standard measure of the bond order parameter  $\psi_6$  [40] for a given particle,  $\psi_6(\mathbf{r}_i) = \frac{1}{N_b} \left| \sum_{m=1}^{N_b} \exp 6i\theta_{mi} \right|$  here  $N_b$  is the number of nearest neighbors of the  $i$ th particle, and  $\theta_{mi}$  is the angle between the  $x$ -axis and the bond joining the  $i$ th particle with the  $m$ th particle. Before we turn to the full statistics of the bond order parameter, it is useful to first look at a coarse-grained measure of this quantity. In analogy to our definition of a local packing fraction, we define a local bond order parameter  $\psi_{6,\text{local}} = (1/N_\Delta) \sum_{i=1}^{N_\Delta} \psi_6(\mathbf{r}_i)$ . The map for  $\psi_{6,\text{local}}$ , corresponding and strongly correlated to the packing shown in Fig. 3(a), is displayed in Fig. 3(c). Such a coarse-grained description shows macroscopically large regions with a very high value of  $\psi_{6,\text{local}}$  consistent with the visual suggestion of crystallinity in Fig. 3(b). Also, note that wherever the soft particles are hyper-packed, the crystallinity is lost, and we have a re-entrant melting scenario [41] highlighted by the dashed black oval in Figs. 3(a) and (c).

Starting from an initial spatially homogeneous particle homogeneous, we have observed that the inhomoge-



neous structures, as illustrated in Fig. 3, emerge over a timescale  $t \approx 5\tau_f$  after the turbulent flow is switched on; please refer to Refs. [35, 36] for an animation of this evolution as well as what happens subsequently when the flow is switched off. In the steady state, the crystalline aggregates are seen to be continuously advected by the underlying flow, and therefore undergo breaking and coalescing at a constant rate as the straining zones evolve with time. Thus, in most cases, a typical crystalline aggregate is transient in nature. To estimate the time scale on which a particular crystalline aggregate persists, we track a subset of particles from our simulations which form a particular crystalline structure. This subset of particles form a crystalline structure at  $t = 47\tau_f$ , with most of the constituents having  $\psi_6 \sim 1$ , and persists for time-scales of the order of a few  $\tau_f$  before *breaking away* to form new crystalline structures [42, 43].

Further, we have also investigated what happens when in steady state conditions, the underlying turbulent flow is suddenly switched off abruptly. The suspended particles should also come to rest, and it indeed does [35, 36], over a timescale determined by  $\tau_p$ . The interesting finding is that the crystalline aggregation in the form of the spatially inhomogeneous structures remain intact; see Figs. S4 (a) and (b) in the Supplementary Material [31] as well as Refs.[35, 36].

The snapshots of Fig. 3 naturally lead us to examine the behaviour of  $\psi_6$  as a function of  $St$  for a reasonably high packing fraction ( $\phi \sim 10\%$ ). Given the non-equilibrium, spatio-temporal variation of the advecting turbulent flow, as discussed above, it is of course natural that all the particles would not arrange themselves in a hexagonal lattice. We therefore look at the *mode*  $[\psi_6]$ , the value of  $\psi_6$  that occurs most frequently amongst all particles and over time. In the non-crystalline phase, the largest number of particles have a value close to 0 whereas in the crystalline phase this value tends to 1.

In Fig. 4(a), we plot  $[\psi_6]$  (black filled circles) as a function of  $St$  and see a remarkable behaviour. For extremely small or large values of the Stokes number,  $[\psi_6] = 0$  whereas for values of  $St$  around 1, where, as seen in Fig. 2, particles show significant preferential concentration,  $[\psi_6] = 1$ . This behaviour is remarkable as it shows a sharp transition between a crystalline and non-crystalline phase (as a function of the Stokes number). Of course such a characterisation makes sense only if there is a macroscopically large fraction of the total particles which show  $[\psi_6]$  as reported in Fig. 4(a). We thus calculate the fraction of particles  $N_{[\psi_6]}/N_p$  (along with their errorbars calculated over time) having  $\psi_6 = [\psi_6]$  (green square symbols). At a practical level,  $\psi_6$  of course varies from 0 to 1; therefore it is convenient for us to bin values of  $\psi_6$ . In particular, we count all particles with values of  $0.0 \leq \psi_6 \leq 0.2$  as  $\psi_6 = 0$  and those in the range  $0.8 \leq \psi_6 \leq 1.0$  as  $\psi_6 = 1.0$ . We have checked that slight variations in this range does not change our results (Fig. 4). Not surprisingly, in the homogeneously dispersed phase ( $St = 0$ ) we find close to 70% of the particles

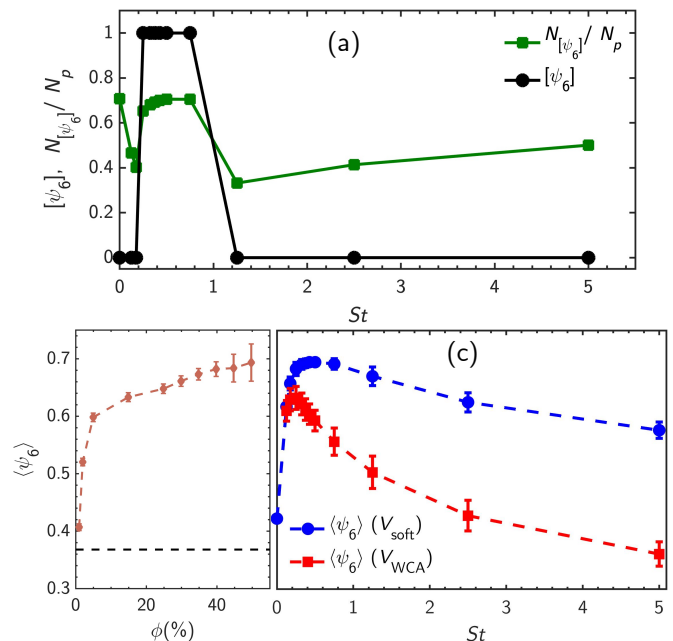


Figure 4. (a)  $\phi = 10\%$ . Variation of  $[\psi_6]$  (black circles), the mode value of  $\psi_6$  computed over all particles in configurations sampled in steady-state, and their associated fraction of particles  $N_{[\psi_6]}/N_p$ , (green squares), with Stokes number  $St$ . (b) For  $St = 1$ , variation of mean value of  $\psi_6$ ,  $\langle \psi_6 \rangle$  with  $\phi$  showing a clear onset of crystalline aggregation, from the dilute random packing (horizontal dashed line). (c) Comparison of  $\langle \psi_6 \rangle$  vs  $St$  for particles interacting via soft harmonic potential, shown with blue circles (for  $\phi = 10\%$ ,  $N_p = 2 \times 10^5$  and  $\sigma = 5 \times 10^{-3}$ ) and WCA potential, shown with red squares (for  $\phi = 25\%$ ,  $N_p = 5 \times 10^5$  and  $\sigma = 4.4 \times 10^{-3}$ ).

are associated with  $\psi_6 = 0.0$ . However as  $0 < St \ll 1.0$ , the spheres tend to weakly cluster leading to a greater variation in  $\psi_6$ . Thus for this range of Stokes numbers, while  $[\psi_6] = 0$ , there is a decrease in  $N_{[\psi_6]}/N_p$  as seen in Fig. 4(a). It is only when the Stokes numbers reach values where particles preferentially concentrate most strongly (see Fig. 2 for comparison), that  $[\psi_6] = 1.0$  and a consequent rise and plateauing of the value of  $N_{[\psi_6]}/N_p$ . Thus, in this crystalline phase where  $[\psi_6] = 1$ , we immediately see (Fig. 4(a)) that a majority of particles arrange themselves in perfect hexagonal order, indicating that indeed there is a dynamical structural transition with Stokes number. For higher Stokes numbers, the particles start to disperse more homogeneously, and the crystalline phase is lost, for reasons discussed before, leading to  $[\psi_6] = 0$ . While for finite Stokes numbers, there are still great variations in the overall values of  $\psi_6$  associated with each particle, as the Stokes number becomes larger and larger, the majority fraction  $N_{[\psi_6]}/N_p$  of those with  $\psi_6 = 0$  increases. The results from our simulations, shown in Fig. 4(a), are consistent with this theoretical understanding of such soft-sphere suspensions.

In the crystalline phase, the variation of the degree of crystallinity  $\langle \psi_6 \rangle$  with the packing fraction is shown

in Fig. 4(b). Clearly, and as conjectured,  $\langle\psi_6\rangle$  increases with  $\phi$ ; remarkably even for very dilute suspension, we do see an average crystalline order with  $\langle\psi_6\rangle$  significantly higher than the value for random packing.

While the two curves in Fig. 4(a) give quantitative evidence for the emergence of a macroscopic crystalline order in an ensemble of particles in a turbulent flow, it is useful to also examine the mean bond order parameter  $\langle\psi_6\rangle$  as a function of the Stokes number. The non-monotonic behaviour of this measure, seen in the curve for  $V_{\text{soft}}$  in Fig. 4(c), is consistent with that seen for  $[\psi_6]$ . Of course the average value does not switch between 0 and 1 because of local fluctuations in the particle arrangement. For the range of Stokes numbers where crystalline structures are observed, we find good evidence for onset of crystallinity by measuring  $\langle\psi_6\rangle$  as a function of  $\phi$  (Fig. 4(c)).

Since the results reported so far have been obtained for soft particles, whereby two particles can overlap/penetrate to mimic deformation at contact for real grains or droplets, it is important to check if this phenomenon is *universal* and, in particular, persists even for hard-core particles, where the repulsive forces will be stronger at contact and thereby affect local packing. In order to do so, we performed simulations where we model the *hard cores* particles via the Weeks-Chandler-Anderson (WCA) inter-particle potential [44] -  $V_{\text{WCA}}(r_{ij}) = 4\epsilon[(\sigma/r_{ij})^{12} - (\sigma/r_{ij})^6] + \epsilon$  for  $r_{ij} \leq 2^{\frac{1}{6}}\sigma$  and 0 otherwise. For this system, we again measure  $\langle\psi_6\rangle$  (in Fig. 4 (b), red squares), with a packing fraction twice as large as that used for soft disks, as a function of  $St$ . Also see Fig. S2 in Supplementary Information [31] for local maps for the WCA particles, similar to what has been shown in Fig. 3 for the harmonic disks. Our measurements show that the degree of maximum crystallinity, at  $St \sim 1$ , is marginally smaller than that for particles with soft interactions and that  $\langle\psi_6\rangle$  falls off faster as a function of  $St$  for the assembly of *hard* disks as compared to *soft* disks. Nevertheless, the basic mechanism of the formation of crystalline aggregates seem to be unchanged even for the extreme case of the WCA potential.

Another consideration is the polydispersity of the granular particles and its effects on the crystalline aggregates [45–47]. To study this we use a bi-disperse assembly of particles with the particle radius ratio of 1.4 [48]. As expected, for such mixtures, the spatial extent of local crystallinity diminishes significantly when compared to the mono-component system (see Fig. S3 of the Supplementary Material [31]). Nevertheless, even for such bi-disperse suspension, dense packings leading to locally jammed structures, induced by the carrier flows, do still occur. Indeed this issue along with the role played by the energy scale  $\epsilon$  needs a detailed study in future.

In conclusion, we have shown that two-dimensional particle-laden turbulent flow, lead to crystalline self-assembly, albeit spatially inhomogeneous, because of the complementary effects of drag-induced preferential concentration and inter-particle interactions [49]. The cen-

tral role played by particle inertia is apparent in the sharp transition between crystalline aggregates as a function of the Stokes number. Our work also shows that elasticity of the particles lead to a modification in the nature of preferential concentration of heavy inertial particles which lie at the heart of several natural and industrial processes.

We also demonstrate that these crystalline aggregates survive even after the turbulent flow is switched off (Fig. S4 of the Supplementary Material [31] and Refs. [35, 36]) by setting  $\mathbf{u}(\mathbf{x}_i, t) = 0$  in Eq. 1. Thus, this provides a route to engineer such inhomogeneous particulate assemblies, for example via drying of the suspending fluid, as it often does in nature. We further note that the chosen value of  $\epsilon$  sets the energy scale such that potential energy is comparable to the kinetic energy as shown in Fig. S3 of the Supplementary Material [31].

It is also important to keep in mind that, given that there have hardly been any studies of particulate structures in a turbulent flow, our work focuses on the most simple and general framework as commonly used in turbulent transport problems. The most important simplification that we have used is to ignore the feedback of the particles on the flow, as well as lubrication forces or the effect of porosity in the packed structures. It has been shown in an earlier work [50] that a one-way coupled model for Stokesian particles is a valid assumption in turbulent flows. Furthermore, it was shown in [29], while studying the problem of elastic collisions in particle-laden turbulent flows, that at least in the small Stokes limit, the effect of short-range lubrication was merely the renormalisation of the effective relaxation time. However, it should be left for future work to actually examine in detail the role of lubrication and porosity in stabilizing such crystalline structures.

Finally, we note that such inhomogeneous crystalline aggregation has recently been observed in assemblies of self-propelled particles [51]. However, the morphology of the clusters in the case of the turbulence led aggregation is perhaps very different, and this needs to be explored further. However, in a broader context, the diverse non-equilibrium routes for such self-assembly opens up fascinating avenues.

## ACKNOWLEDGMENTS

We thank J. R. Picardo and S. Puri for useful suggestions and discussions. JB and SSR acknowledge the support of the Indo-French Centre for Applied Mathematics (IFCAM). SSR acknowledges the support of SERB-DST (India) projects MTR/2019/001553, STR/2021/000023, CRG/2021/002766 and the DAE, Govt. of India, under project no. 12-R&D-TFR-5.10-1100 and project no. RTI4001 PC acknowledges CEFIPRA Grant No. 5604-1 for financial support. This research was supported in part by the International Centre for Theoretical Sciences (ICTS) during a visit of PC for participating in

the program - Entropy, Information and Order in Soft Matter (Code: ICTS/eiosm2018/08). The simulations

were performed on the ICTS clusters *Mowgli Mario*, and *Tetris*, as well as the work stations from the project ECR/2015/000361: *Goopy* and *Bagha*.

- 
- [1] G. M. Whitesides and B. Grzybowski, “Self-assembly at all scales,” *Science* **295**, 2418–2421 (2002).
- [2] L. Scarabelli, M. Coronado-Puchau, J. J. Giner-Casares, J. Langer, and L. M. Liz-Marzán, “Monodisperse gold nanotriangles: size control, large-scale self-assembly, and performance in surface-enhanced raman scattering,” *ACS nano* **8**, 5833–5842 (2014).
- [3] N. A. Clark, A. J. Hurd, and B. J. Ackerson, “Single colloidal crystals,” *Nature* **281**, 57–60 (1979).
- [4] P. N. Pusey and W. Van Meegen, “Phase behaviour of concentrated suspensions of nearly hard colloidal spheres,” *Nature* **320**, 340–342 (1986).
- [5] A. J. Liu and S. R. Nagel, “The jamming transition and the marginally jammed solid,” *Annu. Rev. Condens. Matter Phys.* **1**, 347–369 (2010).
- [6] F. m. c. Boyer, E. Guazzelli, and O. Pouliquen, “Unifying suspension and granular rheology,” *Phys. Rev. Lett.* **107**, 188301 (2011).
- [7] P. Coussot and N. J. Wagner, “The future of suspension rheophysics: comments on the 2008 workshop,” (2009).
- [8] D. Bonn, M. M. Denn, L. Berthier, T. Divoux, and S. Manneville, “Yield stress materials in soft condensed matter,” *Rev. Mod. Phys.* **89**, 035005 (2017).
- [9] M. Doi and D. Chen, “Simulation of aggregating colloids in shear flow,” *The Journal of Chemical Physics* **90**, 5271–5279 (1989).
- [10] J. Vermant and M. J. Solomon, “Flow-induced structure in colloidal suspensions,” *Journal of Physics: Condensed Matter* **17**, R187 (2005).
- [11] M. L. Wells and E. D. Goldberg, “Occurrence of small colloids in sea water,” *Nature* **353**, 342–344 (1991).
- [12] M. L. Wells and E. D. Goldberg, “Colloid aggregation in seawater,” *Marine Chemistry* **41**, 353–358 (1993).
- [13] P. Kepkay, S. Niven, and J. Jellett, “Colloidal organic carbon and phytoplankton speciation during a coastal bloom,” *Journal of plankton research* **19**, 369–389 (1997).
- [14] E. K. Longmire and J. K. Eaton, “Structure of a particle-laden round jet,” *Journal of Fluid Mechanics* **236**, 217–257 (1992).
- [15] R. Monchaux, M. Bourgoin, and A. Cartellier, “Analyzing preferential concentration and clustering of inertial particles in turbulence,” *International Journal of Multiphase Flow* **40**, 1–18 (2012).
- [16] K. Gustavsson and B. Mehlig, “Statistical models for spatial patterns of heavy particles in turbulence,” *Adv. in Phys.* **65**, 1–57 (2016).
- [17] J. Bec, L. Biferale, M. Cencini, A. Lanotte, S. Musacchio, and F. Toschi, “Heavy particle concentration in turbulence at dissipative and inertial scales,” *Phys. Rev. Lett.* **98**, 084502 (2007).
- [18] S. Goto and J. C. Vassilicos, “Sweep-stick mechanism of heavy particle clustering in fluid turbulence,” *Phys. Rev. Lett.* **100**, 054503 (2008).
- [19] J. Chun, D. L. Koch, S. L. Rani, A. Ahluwalia, and L. R. Collins, “Clustering of aerosol particles in isotropic turbulence,” *Journal of Fluid Mechanics* **536**, 219–251 (2005).
- [20] J. Bec, H. Homann, and S. S. Ray, “Gravity-driven enhancement of heavy particle clustering in turbulent flow,” *Phys. Rev. Lett.* **112**, 184501 (2014).
- [21] G. H. Good, P. J. Ireland, G. P. Bewley, E. Bodenschatz, L. R. Collins, and Z. Warhaft, “Settling regimes of inertial particles in isotropic turbulence,” *J. Fluid Mech.* **759**, R3 (2014).
- [22] K. Gustavsson, S. Vajedi, and B. Mehlig, “Clustering of particles falling in a turbulent flow,” *Phys. Rev. Lett.* **112**, 214501 (2014).
- [23] S. Belan, I. Fouxon, and G. Falkovich, “Localization-delocalization transitions in turbophoresis of inertial particles,” *Phys. Rev. Lett.* **112**, 234502 (2014).
- [24] F. De Lillo, M. Cencini, S. Musacchio, and G. Boffetta, “Clustering and turbophoresis in a shear flow without walls,” *Phys. Fluids* **28**, 035104 (2016).
- [25] D. Mitra, N. E. L. Haugen, and I. Rogachevskii, “Turbophoresis in forced inhomogeneous turbulence,” *The European Physical Journal Plus* **133**, 1–8 (2018).
- [26] J. Bec, S. S. Ray, E. W. Saw, and H. Homann, “Abrupt growth of large aggregates by correlated coalescences in turbulent flow,” *Phys. Rev. E* **93**, 031102(R) (2016).
- [27] X.-Y. Li, A. Brandenburg, G. Svensson, N. E. Haugen, B. Mehlig, and I. Rogachevskii, “Effect of turbulence on collisional growth of cloud droplets,” *Journal of the Atmospheric Sciences* **75**, 3469–3487 (2018).
- [28] A. Choudhary, D. Venkataraman, and S. S. Ray, “Effect of inertia on model flocks in a turbulent environment,” *EPL (Europhysics Letters)* **112**, 24005 (2015).
- [29] J. Bec, M. Stefano, and S. S. Ray, “Sticky elastic collisions,” *Phys. Rev. E* **87**, 063013 (2013).
- [30] C. S. O’Hern, L. E. Silbert, A. J. Liu, and S. R. Nagel, “Jamming at zero temperature and zero applied stress: The epitome of disorder,” *Phys. Rev. E* **68**, 011306 (2003).
- [31] See Supplemental Material at [URL will be inserted by publisher] for additional details.
- [32] D. J. Durian, “Foam mechanics at the bubble scale,” *Phys. Rev. Lett.* **75**, 4780–4783 (1995).
- [33] S. S. Ray, D. Mitra, P. Perlekar, and R. Pandit, “Dynamic multiscaling in two-dimensional fluid turbulence,” *Phys. Rev. Lett.* **107**, 184503 (2011).
- [34] G. Boffetta, R. E. Ecke, et al., “Two-dimensional turbulence,” *Annual review of fluid mechanics* **44**, 427–451 (2012).
- [35] See Supplemental Movie at [URL will be inserted by publisher] for an animation showing the evolution of  $\phi_{\text{local}}$  and  $\psi_{\text{local}}^6$  as well as how the dynamics freezes on switching off the flow.
- [36] See <https://youtu.be/uTazvh1ETD8> for an animation showing the evolution of  $\phi_{\text{local}}$  and  $\psi_{\text{local}}^6$  as well as how the dynamics freezes on switching off the flow.
- [37] A. J. Petersen, L. Baker, and F. Coletti, “Experimental study of inertial particles clustering and settling in homogeneous turbulence,” *Journal of Fluid Mechanics* **864**,

- 925–970 (2019).
- [38] C. Radin, “Random close packing of granular matter,” *Journal of Statistical Physics* **131**, 567–573 (2008).
- [39] S. Henkes, Y. Fily, and M. C. Marchetti, “Active jamming: Self-propelled soft particles at high density,” *Phys. Rev. E* **84**, 040301 (2011).
- [40] P. J. Steinhardt, D. R. Nelson, and M. Ronchetti, “Bond-orientational order in liquids and glasses,” *Phys. Rev. B* **28**, 784–805 (1983).
- [41] M. Zu, J. Liu, H. Tong, and N. Xu, “Density affects the nature of the hexatic-liquid transition in two-dimensional melting of soft-core systems,” *Phys. Rev. Lett.* **117**, 085702 (2016).
- [42] See Supplemental Movie at [URL will be inserted by publisher] for an animation showing the formation and breaking up of a crystalline aggregate,.
- [43] See <https://youtu.be/BzQPgpQPW5Y> for an animation showing the formation and breaking up of a crystalline aggregate,.
- [44] J. D. Weeks, D. Chandler, and H. C. Andersen, “Role of repulsive forces in determining the equilibrium structure of simple liquids,” *The Journal of chemical physics* **54**, 5237–5247 (1971).
- [45] J. Russo and N. B. Wilding, “Disappearance of the hexatic phase in a binary mixture of hard disks,” *Phys. Rev. Lett.* **119**, 115702 (2017).
- [46] P. Sampedro Ruiz, Q.-l. Lei, and R. Ni, “Melting and re-entrant melting of polydisperse hard disks,” *Communications Physics* **2**, 1–6 (2019).
- [47] P. Sampedro Ruiz and R. Ni, “Effect of particle size distribution on polydisperse hard disks,” *The Journal of Chemical Physics* **153**, 174501 (2020).
- [48] C. S. O’hern, L. E. Silbert, A. J. Liu, and S. R. Nagel, “Jamming at zero temperature and zero applied stress: The epitome of disorder,” *Physical Review E* **68**, 011306 (2003).
- [49] A recent experiment on particles settling under gravity show signatures of crystalline phases in incompressible flows (A. Petersen, L. Baker, and F. Coletti, *J. Fluid Mech.* **864**, 925-970 (2019)),.
- [50] E.-W. Saw, G. P. Bewley, E. Bodenschatz, S. S. Ray, and J. Bec, “Extreme fluctuations of the relative velocities between droplets in turbulent airflow,” *Phys. Fluids* **26**, 111702 (2014).
- [51] J. Palacci, S. Sacanna, A. P. Steinberg, D. J. Pine, and P. M. Chaikin, “Living crystals of light-activated colloidal surfers,” *Science* **339**, 936–940 (2013).



# Supplemental Information for “Turbulent Route to Two-Dimensional Soft Crystals”

Mohit Gupta,<sup>1,2,\*</sup> Pinaki Chaudhuri,<sup>3,†</sup> Jérémie Bec,<sup>4,5,‡</sup> and Samriddhi Sankar Ray<sup>1,§</sup>

<sup>1</sup>*International Centre for Theoretical Sciences, Tata  
Institute of Fundamental Research, Bangalore 560089, India*

<sup>2</sup>*School of Physics and Astronomy, University of Minnesota,  
Minneapolis, Minnesota 55455, USA*

<sup>3</sup>*The Institute of Mathematical Sciences, CIT Campus, Taramani, Chennai 600 113, India*

<sup>4</sup>*Université Côte d’Azur, Inria, CNRS, Cemef, 06902 Sophia-Antipolis, France.*

<sup>5</sup>*MINES ParisTech, PSL Research University,  
CNRS, CEMEF, 06904 Sophia-Antipolis, France*

arXiv:1812.06487v2 [physics.flu-dyn] 9 Dec 2022

---

\* mohit.gupta9607@gmail.com

† pinakic@imsc.res.in

‡ jeremie.bec@mines-paristech.fr

§ samriddhisankarray@gmail.com

## I. SUPPLEMENTARY FIGURES

### A. $D_2$ at higher packing fractions

The minimum value of obtained  $D_2$  as a function of  $St$  increases as packing fraction increases. To study weather the minim in the  $D_2$  disappears at a high enough packing fraction we show data obtained at higher packing fractions in Fig. S1.

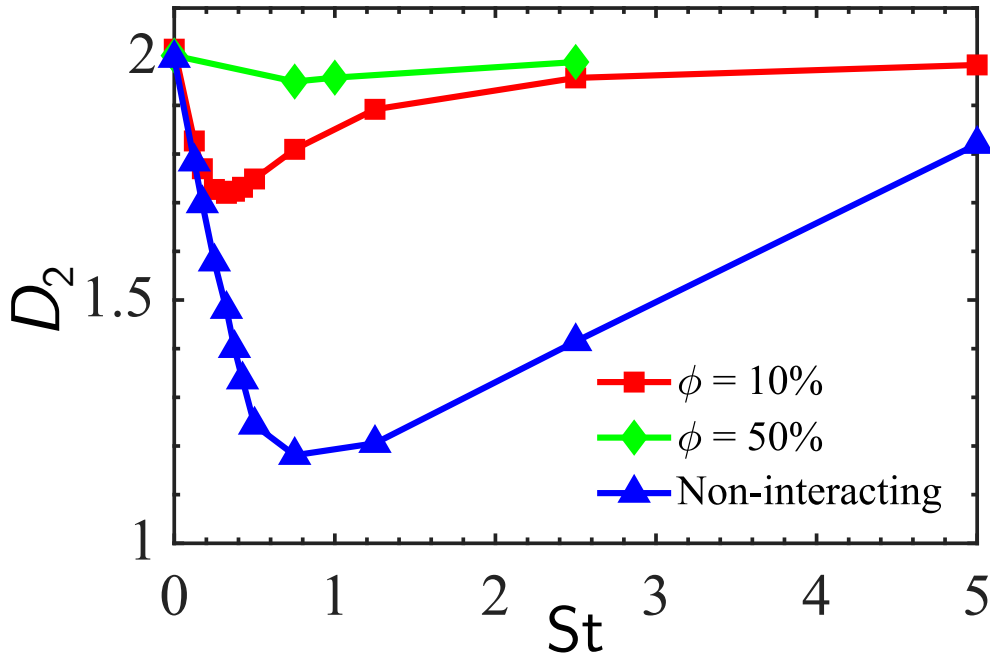


FIG. S1. *Soft Harmonic disks*. Correlation dimension  $D_2$  vs  $St$  for non-interacting (blue triangles) and interacting particles, where  $N_p$  is fixed and  $\phi$  is varied by changing the particle diameter. (The error-bars are smaller than the symbols size).

### B. Hard-core particles: Weeks-Chandler-Anderson Potential

To study the response of an assembly of particles, with hard-core like interactions, we consider a monodisperse system where particles interact via the Weeks-Chandler-Anderson (WCA) potential (see main text for the functional form). We study the structures at  $\phi = 25\%$ , using  $N_p = 5.0 \times 10^5$  and  $\sigma = 0.0044$  with effective diameter being  $2^{1/6} \times \sigma = 0.005$ . As illustrated in Fig.S2, we observe that the degree of crystallisation is less compared to the case of *harmonic disks*.

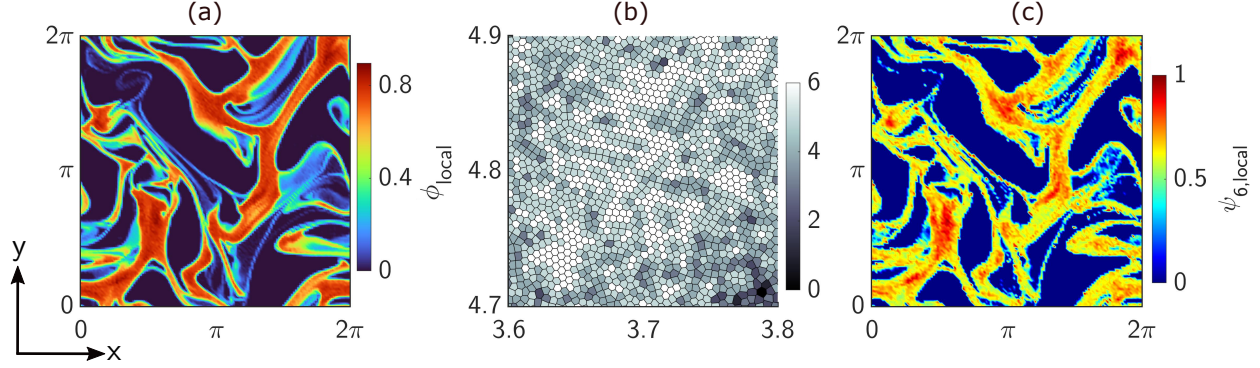


FIG. S2.  $\phi = 25\%$ . Particles interacting via WCA potential. (a) Local packing fraction field  $\phi_{\text{local}}$  for the suspended grains, with  $St \sim 1$ . (b) The Voronoi tessellation along with the coordination number  $z$  of each particle, shown as greyscale for a zoomed-in region having large  $\psi_{6,\text{local}}$  indicates a weak crystalline order compared to the soft harmonic potential. Color-bar shows number of sides of each Voronoi cell. (c) Corresponding map for the local bond order parameter  $\psi_{6,\text{local}}$ .

### C. Bi-disperse assembly of soft particles

To study the effect of size dispersity on the structure formation, we perform simulations of a bi-disperse (50:50) system, with a size ratio of 1.4. Here particles interact via the soft harmonic potential. We study the structures using  $N_p = 10.0 \times 10^5$ , with the two sizes being  $\sigma_1 = 0.005$  and  $\sigma_2 = 0.007$ , giving  $\phi = 60\%$ . As illustrated in Fig.S3, we observe that the spatial extent of crystallisation is significantly less compared to the monodisperse case. To isolate the effect of soft-particle interactions we set the Stokes number to be the same for both radius, which is equivalent to a change in the density of the particles.

### D. Particle assembly with $\mathbf{u} = 0$

We have looked at the particle assembly after we *turn off* the flow, i.e we have set  $\mathbf{u} = 0$  after the system has reached steady state. As shown in the supplementary movie and seen from Fig. S4 (c), the system freezes as mean kinetic energy  $\langle E_k \rangle \sim 0$  and mean potential energy  $\langle E_p \rangle \sim 0$  in time  $t > \tau_p$ . As particles come to a halt the order in the system remains stable (Fig. S4 (b)).

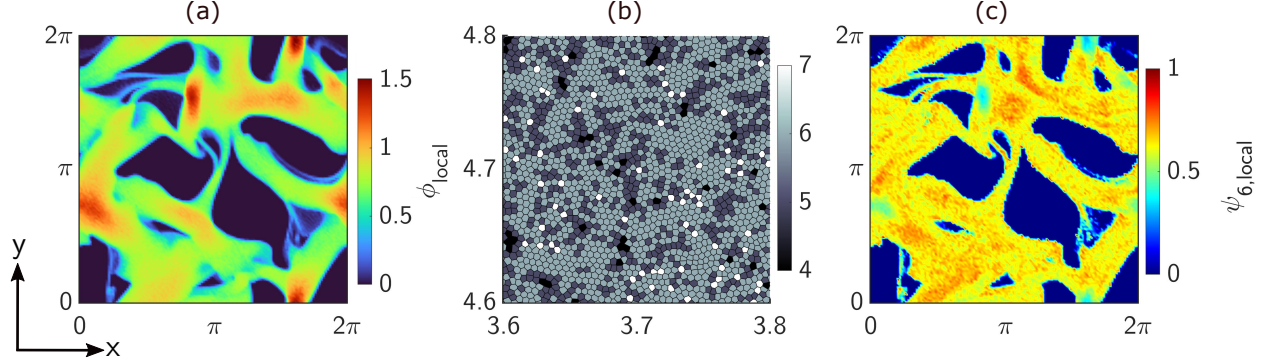


FIG. S3.  $\phi = 60\%$ . Bi-disperse assembly of particles interacting via soft potential. (a) Local packing fraction field  $\phi_{\text{local}}$  for the suspended grains, with  $St \sim 1$ . (b) The Voronoi tessellation along with the coordination number  $z$  of each particle, shown as grayscale for a zoomed-in region having large  $\psi_{6,\text{local}}$ . Color-bar shows number of sides of each Voronoi cell. (c) Corresponding map for the local bond order parameter  $\psi_{6,\text{local}}$  indicates a weak crystalline order compared to the mono-disperse solution.

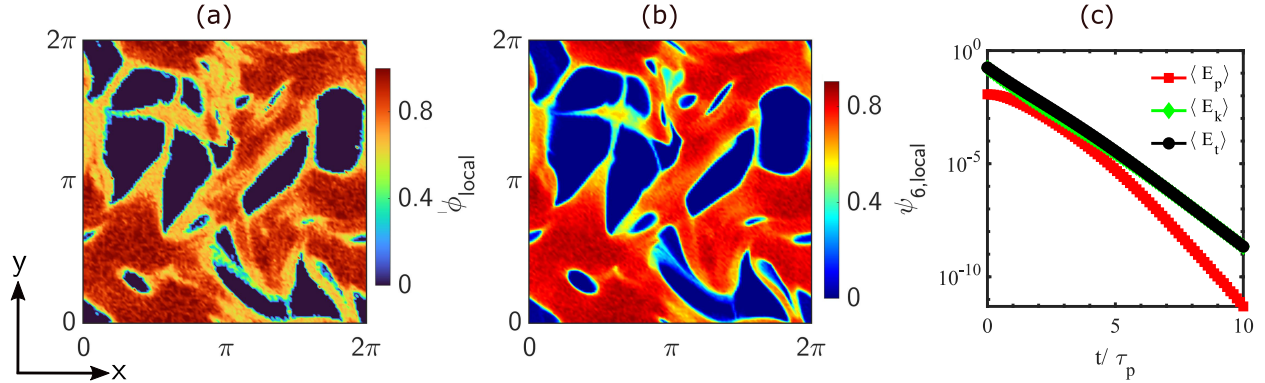


FIG. S4.  $\phi = 50\%$ . Particle assembly after the flow is abruptly stopped. (a) Local packing fraction field  $\phi_{\text{local}}$  for the suspended grains, with  $St \sim 1$ . (b) Corresponding map for the local bond order parameter  $\psi_{6,\text{local}}$ . (c) Mean kinetic energy  $\langle E_k \rangle$  (green circles), mean potential energy  $\langle E_p \rangle$  (red circles) and total energy  $\langle E_t \rangle$  (black circles) of particles as function of time after the flow is stopped.

## II. SUPPLEMENTARY MOVIE

### A. Particle Evolution

We show time evolution of the system of  $N_p = 10^6$  particles, having diameter  $\sigma = 5 \times 10^{-3}$  which gives  $\phi = 50\%$ , interacting via harmonic interactions, with  $St = 1$ . We start from



a spatially homogeneous distribution of particles. In the movie, the left panel shows the local packing fraction field  $\phi_{\text{local}}$  for the suspended grains, and the right panel shows the corresponding map for the local bond order parameter  $\psi_{6,\text{local}}$ . As the system evolves, for  $t > \tau_f$ , we obtain preferentially concentrated state where particles are concentrated in the straining zones, causing large density fluctuations. This leads to local crystalline order in the system as we can see from the value of  $\psi_{6,\text{local}}$ .

We *turn off* the flow at  $t = 75\tau_f$  and it can be seen that the system *freezes* and the particles obtain there equilibrium positions in  $t > \tau_p$ . The video is also available at [1].

## B. Cluster time scale

We show time evolution of a subset of particles from our simulations ( $N_p = 10^6$ ,  $\sigma = 5 \times 10^{-3}$ ). The particles are colored according to their instantaneous  $\psi_6$ , with  $\text{St} = 1$ . As these particles move they form a crystalline structure at  $t = 47\tau_f$ . After a few  $\tau_f$  this structure breaks up and constituent particles evolve in time to form different clusters. The video is also available at [2].

---

[1] <https://youtu.be/uTazvh1ETD8>.

[2] <https://youtu.be/BzQPgpQPW5Y>.